Nonresonant Axion-Like Particle Searches at the LHC: Implications for Vector Boson Scattering

J. Bonilla,[a,b] **I. Brivio,**[c] **J. Machado**[a,b] **and J. F. de Trocóniz**[a,*]

[a]*Dpto. de Física Teórica, Universidad Autónoma de Madrid,*
E28049 Madrid, Spain

[b]*Instituto de Física Teórica IFT,*
E28049 Madrid, Spain

[c]*Institut für Teoretische Physik, Universität Heidelberg,*
D69120 Heidelberg, Germany

E-mail: jesus.bonilla@uam.es, brivio@thphys.uni-heidelberg.de,
jonathan.machado@uam.es, jorge.troconiz@uam.es

We discuss nonresonant axion-like particle (ALP) searches in diboson production at the LHC, a collider probe for ALPs which takes advantage of the derivative nature of their interactions with Standard Model particles; here ALPs participate as off-shell mediators in the scattering process. The power of this novel type of search has been tested with gluon-initiated diboson nonresonant production processes, using CMS and ATLAS Run 2 data, probing previously unexplored areas of the ALP parameter space. In addition, new studies on nonresonant ALP-mediated vector boson scattering (VBS) and preliminary results based on recently published CMS data are presented. Expectations for LHC Run 3 and HL-LHC are derived.

*** The European Physical Society Conference on High Energy Physics (EPS-HEP2021), ***
*** 26-30 July 2021 ***
*** Online conference, jointly organized by Universität Hamburg and the research center DESY ***

---

*Speaker

1. Introduction

Several extensions of the standard model (SM) predict the existence of new particles with enhanced couplings to a pair of electroweak (EWK) bosons $V = W, Z, \gamma$. Searching for signals beyond the SM in diboson final states is a major goal for the ATLAS and CMS experiments.

Axion-like particles (ALPs) [1, 2] are neutral pseudoscalar bosons with derivative interactions with SM particles, and often appear in extensions of the SM. ALP interactions can be parameterized using the model-independent approach of effective field theories (EFTs). In this report we focus on the linear EFT implementation and adopt the definitions of Refs. [3, 5]. The ALP couplings with SM particles are proportional to a Wilson coefficient c and inversely proportional to the new physics energy scale f_a. Classical searches for ALPs at colliders consider their couplings to photons and gluons. The coefficient of the gluon coupling is $c_{\widetilde{G}}$. More recently, interest has extended to consider ALP couplings to EWK bosons: ZZ, WW, and $Z\gamma$ [3]. At LO, all these and the coupling to photons are related by gauge symmetry to two basic electroweak couplings: $c_{\widetilde{W}}$ and $c_{\widetilde{B}}$. Here, small couplings of the ALP to fermions are neglected.

Colliders allow searches in a wide range of ALP masses and couplings [3–5]. An interesting diboson production mechanism is gluon-initiated nonresonant ALP-mediated scattering; the ALP is an off-shell mediator in the s-channel $2 \rightarrow 2$ scattering processes [5]. These channels are sensitive to the product of the ALP coupling to gluons and the relevant coupling to dibosons. These searches have been identified as promising because the cross sections are large enough to significantly constrain the theoretical models using the full Run 2 LHC data set. The derivative interactions enhance the cross section at large diboson invariant masses, $\sqrt{\hat{s}}$. In the ALP off-shell regime $\sqrt{\hat{s}} \gg m_a, m_V$, the partonic cross section for $gg \rightarrow a^* \rightarrow V_1 V_2$ grows as $\hat{s}/f_a^4$. Such energy dependence is only valid as long as the energies probed in the scattering process are smaller than f_a. The nonresonant cross sections and kinematical distributions are found to be independent of the ALP mass from arbitrarily light masses up to masses of the order of 100 GeV. The experimental strategy is to look for deviations with respect to SM expectations in the tails of the bosons transverse momenta or diboson mass distributions.

ALP coupling limits derived from reinterpretations of CMS and ATLAS Run 2 measurements can be found in Refs. [5, 6]. CMS has recently published the first dedicated search for nonresonant ALP-mediated ZZ production in semileptonic final states at the LHC [7]. These analyses probe previously unexplored areas of the ALP parameter space. Combining all results, a limit on $c_{\widetilde{G}}/f_a \lesssim 0.03$ TeV^{-1} is established, for $c_{\widetilde{W}}/f_a$ or $c_{\widetilde{B}}/f_a \geq 1$ TeV^{-1}, the region of ALP EWK couplings later explored in this report.

In this report, we focus on nonresonant ALP-mediated vector boson scattering (VBS). Nonresonant ALP-mediated EWK VBS diboson production is sensitive to the ALP electroweak couplings independently of the ALP coupling to gluons. The LO ALP-mediated EWK VBS Feynman diagrams are depicted in Fig. 1. They contain an offshell ALP interchanged in the t-channel for all final states; s-channel is relevant only for the ZZ, $W^\pm W^\mp$ and $Z\gamma$ final states. ALP triboson production in the same final states is efficiently supressed with a cut on the dijet invariant mass $m_{q_1' q_2'} > 120$ GeV.

ATLAS and CMS have recently published Run 2 VBS diboson production measurements. These analyses allow first comparison to the data, calibration of the simulation tools, and calculation of educated predictions for higher LHC luminosities.
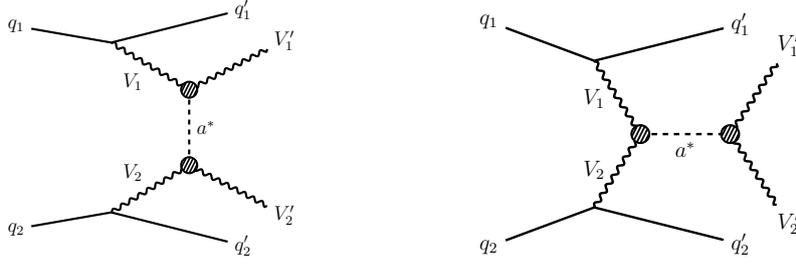
Figure 1: LO ALP-mediated EWK VBS *t*-channel (left) and *s*-channel (right) Feynman diagrams.

2. ALP-mediated EWK VBS Simulation and Analysis

Simulated signals of non-resonant ALP-mediated EWK VBS diboson production are generated with MadGraph5_aMC@NLO 2.8.2 [8]. In the EFT linear model $q_1 q_2 \rightarrow q_1' q_2' V_1' V_2'$ events (Fig. 1) are generated at LO in the ALP and EWK couplings and at zeroth order in the QCD coupling with $c_{\widetilde{W}}/f_a = c_{\widetilde{B}}/f_a = 1 \text{ TeV}^{-1}$ and an ALP mass of 1 MeV. Considered initial state (anti)quarks are up, down, strange, and charm. We generate separate samples for pure ALP-mediated production and the interference between the ALP and the SM EWK VBS production. In addition, we generate full samples of the ALP signals and their interferences with photophobic couplings $c_{\widetilde{W}}/f_a = 1 \text{ TeV}^{-1}$ and $c_{\widetilde{B}}/f_a = -t_W^2 \text{ TeV}^{-1}$, where t_W is the tangent of the Weinberg angle, and an ALP mass of 1 MeV. The corresponding cross sections at $\sqrt{s} = 13$ TeV are summarized in Table 1. There is a 11% systematic uncertainty in the size of the cross sections related to the renormalization and factorization scales and a 4% systematic uncertainty related to the PDFs. Samples corresponding to other choices of the $c_{\widetilde{W}}/f_a$ and $c_{\widetilde{B}}/f_a$ couplings are obtained from the previous ones using the MadGraph5 event reweighting tool [9]. ALP-mediated QCD VBS diboson production is neglected.

Consistency of the EFT description implies that the diboson invariant masses should be smaller that the cutoff scale f_a. ALP events with diboson invariant masses smaller than 4 (2) TeV represent > 99% (85%, respectively) of the total generated samples.

Analogously, SM EWK VBS diboson background events are generated with MadGraph5 at LO in the EWK couplings and zeroth order in the QCD coupling. This is an irreducible source of background for the analysis. Cross sections at $\sqrt{s} = 13$ TeV are presented in Table 1.

Table 1: EWK VBS SM background and ALP cross sections at $\sqrt{s} = 13$ TeV for two benchmark $c_{\widetilde{W}}/f_a = 1 \text{ TeV}^{-1}$ cases and dijet invariant mass $m_{q_1' q_2'} > 120$ GeV; expected number of ALP events ($c_{\widetilde{W}}/f_a = c_{\widetilde{B}}/f_a = 1 \text{ TeV}^{-1}$) after CMS selection and corresponding integrated luminosities.

	SM EWK VBS (fb)	ALP $c_{\widetilde{W}}/f_a = c_{\widetilde{B}}/f_a$ signal / interf. (fb)	ALP photophobic signal / interf. (fb)	#events CMS	Int. luminosity (fb^{-1})
ZZ	100	42 / -13	18 / -9	9.3 / -3.2	137
$W^\pm Z$	390	18 / 1.7	24 / -0.1	4.2 / 0.05	137
$W^\pm W^\pm$	250	16 / -4.0		18 / -5.5	137
$W^\pm \gamma$	990	29 / 4.3	5.4 / 1.7	3.6 / -0.04	36
$Z\gamma$	390	11 / 0.3	21 / -9	15 / -0.07	137

For all the simulated samples in the analysis, parton showering, hadronization and decays are

described by interfacing the event generators with PYTHIA 8 [10]. Massive EWK bosons V_1' and V_2' are forced to decay leptonically (electrons and muons). The parton distribution functions (PDFs) of the colliding protons are given by the NNPDF 3.0 PDF set [11] for all simulated samples. No additional pileup pp interactions were added. All samples were processed through a simulation of the CMS detector and reconstruction of the experimental objects using DELPHES 3 [12], including FastJet [13] for the clustering of anti-k_T jets with a distance parameter of 0.4 (AK4 jets).

We use the selections and results recently published by the CMS Collaboration searching for VBS production of ZZ [14], same sign $W^\pm W^\pm$ [15], $W^\pm Z$ [15], $W^\pm \gamma$ [16] and $Z\gamma$ [17] bosons in association with two forward jets. The five channels use leptonic (electron and muon) decays of the W and Z bosons in the final state. The expected numbers of ALP events after CMS selection for benchmark case $c_{\widetilde{W}}/f_a = c_{\widetilde{B}}/f_a = 1$ TeV^{-1} and corresponding integrated luminosities are presented in Table 1.

We take into account the differences between our generation and simulation procedure and the ones used by the CMS experiment comparing the predicted numbers of events after selection cuts for the SM EWK VBS $q_1 q_2 \rightarrow q_1' q_2' V_1' V_2'$ processes. We define a scale-factor as the ratio of the number of CMS expected events and the number of expected events delivered by our generation and simulation procedure. The same scale factors were then applied to the predictions for pure ALP-mediated EWK VBS and ALP-SM interference simulated samples. A systematic uncertainty of 16% on the simulated ALP event yields is assigned.

The number of events for the data and for the SM background predictions are taken from the CMS experimental publications. Systematic uncertainties affecting the SM background distributions, taken from the CMS publications as well, are applied to the SM background and the ALP signal contributions in the final fits. Systematic uncertainties are considered uncorrelated among the different diboson channels.

3. Results

Signal efficiencies for the various diboson channels range from 0.2% to 0.9%, including leptonic branching fractions.

Results are extracted from a maximum likelihood fit of signal and background to the diboson invariant mass (ZZ, $W^\pm \gamma$ and $Z\gamma$) or transverse mass ($W^\pm Z$ and $W^\pm W^\pm$) distributions, individually and simultaneously in all the experimental channels used in the analysis. The signal includes both the contribution of a pure ALP-mediated EWK VBS process and its interference with the SM EWK VBS process. The expected signal diboson invariant mass or transverse mass distributions are parameterized in the ($c_{\widetilde{W}}/f_a$, $c_{\widetilde{B}}/f_a$) plane with a fourth- and a second-degree polynomial for the pure ALP-mediated EWK VBS signal and for its interference, respectively. The systematic uncertainties discussed previously are included as nuisance parameters in the maximum likelihood fit, and the background-only hypothesis is tested against the combined background and signal hypothesis.

No significant excess is observed with respect to the SM expectations. ALP couplings $c_{\widetilde{W}}/f_a$ and $c_{\widetilde{B}}/f_a$ are considered excluded at 95% confidence level (CL) when the negative log likelihood (NLL) of the combined background and signal hypothesis exceeds in 3.84/2 units the NLL of the background-only hypothesis. We define the ALP mass range where our results are considered valid
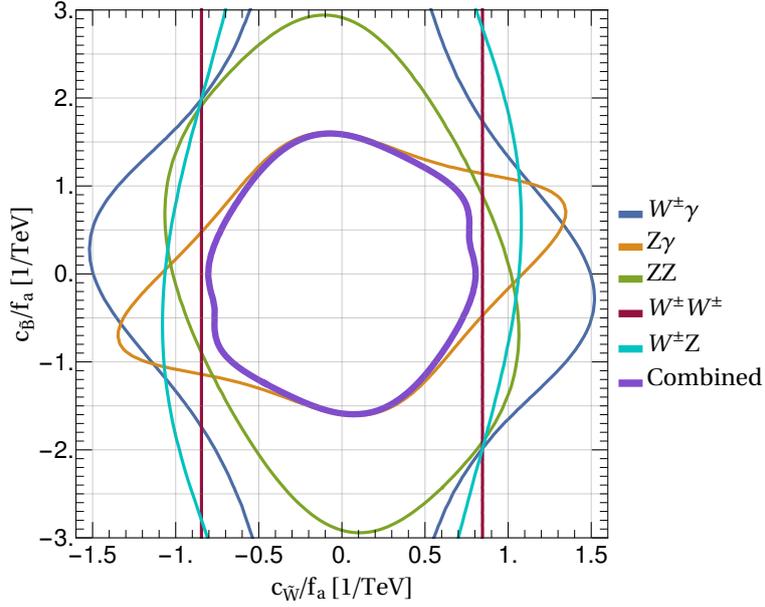
Figure 2: Observed 95% CL upper limits in the $(c_{\widetilde{W}}/f_a,\ c_{\widetilde{B}}/f_a)$ plane using the data of the Run 2 CMS publications, corresponding to the integrated luminosities detailed in Table 1, individually for the five different experimental channels considered (ZZ (green), $W^\pm W^\pm$ (red) and $W^\pm Z$ (light blue), $W^\pm \gamma$ (dark blue) and $Z\gamma$ (orange)), and for its combination (purple). The limits are valid for large f_a ($f_a \gtrsim 4$ TeV) and $m_a \lesssim 100$ GeV.
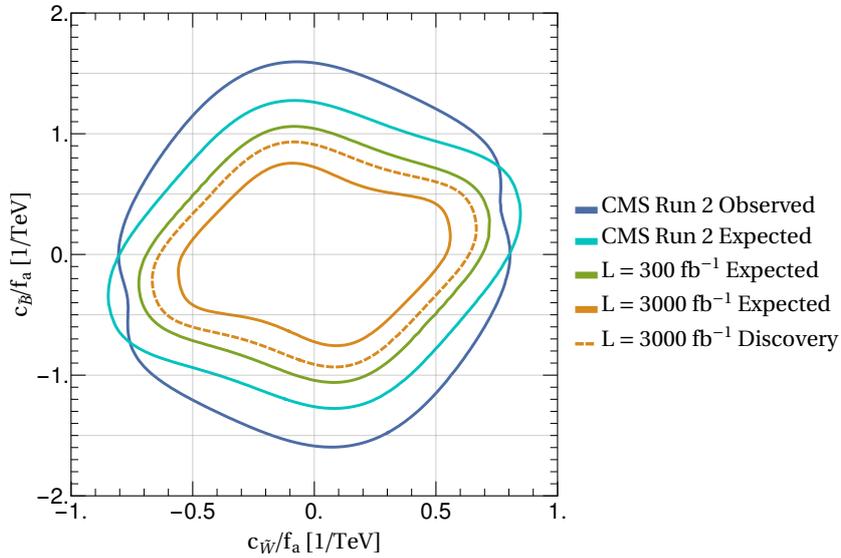
Figure 3: Combined 95% CL upper limits in the $(c_{\widetilde{W}}/f_a,\ c_{\widetilde{B}}/f_a)$ plane: the observed (dark blue) and expected (light blue) limits using the integrated luminosities detailed in Table 1 of the Run 2 CMS publications, and the expected limits for similar experimental analyses at $\sqrt{s} = 14$ TeV with integrated luminosities of 300 fb^{-1} (green) and 3000 fb^{-1} (orange full). The orange dashed curve shows the combined five sigma discovery limits at $\sqrt{s} = 14$ TeV for an integrated luminosity of 3000 fb^{-1}. The limits are valid for large f_a ($f_a \gtrsim 4$ TeV) and $m_a \lesssim 100$ GeV.

as the region where the ALP cross sections diverge by less than 10% from their asymptotic values, $m_a \lesssim 100$ GeV.

Figure 2 shows the observed 95% CL upper limits in the $(c_{\widetilde{W}}/f_a,\ c_{\widetilde{B}}/f_a)$ plane using the data of the full Run 2 CMS publications, corresponding to the integrated luminosities detailed in Table 1, individually for the five different experimental channels considered and for its combination. These limits are valid for large f_a ($f_a \gtrsim 4$ TeV) and $m_a \lesssim 100$ GeV.

Figure 3 shows combined 95% CL upper limits in the $(c_{\widetilde{W}}/f_a,\ c_{\widetilde{B}}/f_a)$ plane: the observed and expected limits using the integrated luminosities detailed in Table 1 of the Run 2 CMS publications, and the expected limits for similar experimental analyses at $\sqrt{s} = 14$ TeV with integrated luminosities of 300 fb^{-1} and 3000 fb^{-1}, representative of the datasets to be accumulated at the end of LHC Run 3 and HL-LHC, respectively. In addition, the combined five sigma discovery limits at $\sqrt{s} = 14$ TeV are presented for an integrated luminosity of 3000 fb^{-1}. These limits are valid for large f_a ($f_a \gtrsim 4$ TeV) and $m_a \lesssim 100$ GeV.

We encourage our colleagues in the ATLAS and CMS Collaborations to perform dedicated ALP-mediated EWK VBS searches at LHC Run 3 and HL-LHC.

References

[1] H. Georgi, D. B. Kaplan, and L. Randall, Phys. Lett. **169B** (1986) 73.

[2] K. Choi, K. Kang, and J. E. Kim, Phys. Lett. B **181** (1986) 145.

[3] I. Brivio, et al., Eur. Phys. J. C **77** (2017) 572.

[4] M. Bauer, M. Neubert, and A. Tahm, JHEP **12** (2017) 044.

[5] M. B. Gavela, J. M. No, V. Sanz, and J. F. de Trocóniz, Phys. Rev. Lett. **124** (2020) 051802.

[6] S. Carra, et al., arXiv:2106.10085, 2021.

[7] CMS Collaboration, CMS Physics Analysis Summary CMS-PAS-B2G-20-013, 2021.

[8] J. Alwall, et al., JHEP **07** (2014) 079.

[9] P. Artoisenet, et al., JHEP **12** (2010) 068.

[10] T. Sjöstrand, et al., Comput. Phys. Commun. **191** (2015) 159.

[11] NNPDF Collaboration, Eur. Phys. J. C **04** (2015) 040.

[12] DELPHES 3 Collaboration (J. de Favereau, et al.), JHEP **1402** (2014) 057.

[13] M. Cacciari, G. P. Salam, and G. Soyez, Eur. Phys. J. C **72** (2012) 1896.

[14] CMS Collaboration (A. M. Sirunyan, et al.), Phys. Lett. B **812** (2020) 135992.

[15] CMS Collaboration (A. M. Sirunyan, et al.), Phys. Lett. B **809** (2020) 135710.

[16] CMS Collaboration (A. M. Sirunyan, et al.), Phys. Lett. B **811** (2020) 135988.

[17] CMS Collaboration (A. Tumasyan, et al.), Phys. Rev. D **104** (2021) 072001.